Title

Fate mapping of neural stem cell niches reveals distinct origins of human cortical astrocytes

Authors

Allen, Denise E
Donohue, Kevin C
Cadwell, Cathryn R
et al.

Peer reviewed

Fate mapping of neural stem cell niches reveals distinct Origins of human cortical astrocytes

Denise E Allen[1,2,3,4],

Kevin C Donohue[2,5,6,7,8],

Cathryn R Cadwell[9],

David Shin[1,2,3,4],

Matthew G Keefe[1,2,3,4],

Vikaas S Sohal[2,7,8],

Tomasz J Nowakowski[1,2,3,4,7,*]

[1]Department of Anatomy, The University of California San Francisco, San Francisco, USA

[2]Department of Psychiatry and Behavioral Sciences, The University of California San Francisco, San Francisco, USA

[3]Department of Neurological Surgery, The University of California San Francisco, San Francisco, USA

[4]Eli and Edythe Broad Center for Regeneration Medicine and Stem Cell Research, The University of California San Francisco, San Francisco, USA

[5]School of Medicine, The University of California San Francisco, San Francisco, USA

[6]Center for Integrative Neuroscience, The University of California San Francisco; San Francisco, USA

[7]Weill Institute for Neurosciences, The University of California San Francisco; San Francisco, USA

[8]Kavli Institute for Fundamental Neuroscience, The University of California San Francisco, San Francisco, USA

[9]Department of Pathology, The University of California San Francisco, San Francisco, USA

Abstract

Progenitors of the developing human neocortex reside in the ventricular and outer subventricular zones (VZ and OSVZ, respectively). However, whether cells derived from these niches have similar developmental fates is unknown. By performing fate mapping in primary human tissue, we demonstrate that astrocytes derived from these niches populate anatomically distinct layers. Cortical plate astrocytes emerge from VZ progenitors and proliferate locally, while putative

*Corresponding author. tomasz.nowakowski@ucsf.edu.

white matter astrocytes are morphologically heterogeneous and emerge from both VZ and OSVZ progenitors. Furthermore, via single-cell sequencing of morphologically defined astrocyte subtypes using Patch-seq, we identify molecular distinctions between VZ- derived cortical plate astrocytes and OSVZ- derived white matter astrocytes that persist into adulthood. Together, our study highlights a complex role for cell lineage in the diversification of human neocortical astrocytes.

One Sentence Summary:

Both germinal niches of the developing human cortex give rise to neurons and glia, but contribute spatially, morphologically, and molecularly distinct astrocyte subtypes.

Radial glia serve as the neural stem cells of the developing neocortex (1, 2). During midgestation in humans, radial glia can be further classified as either CRYAB$^+$ truncated radial glia (tRG) that lose their pial contact and remain in the ventricular zone (VZ) (3), or HOPX$^+$ outer radial glia (oRG) that lose their ventricular contact and reside in the outer subventricular zone (OSVZ) alongside neuronal intermediate progenitor cells (IPCs) (4–6)(7–10). These VZ and OSVZ stem cell niches can also be further distinguished based on their extracellular matrix components (7, 11) and signaling pathway activation (11). Prior studies have shown that progenitor cells residing in the OSVZ contribute to cortical neurogenesis (9, 11, 12), astrogliogenesis (13), and oligodendrocytes (14), but the cells generated by human VZ progenitors are less well-characterized (3). tRG cells emerge at the onset of astrogliogenesis (3), suggesting that they could also contribute to the cortical astrocyte pool. To determine whether both VZ and OSVZ progenitors contribute cortical astrocytes, we performed fate mapping of the human VZ and OSVZ. Our study revealed that VZ and OSVZ progenitors give rise to spatially, morphologically, and molecularly distinct subpopulations of astrocytes, highlighting the complexity of developmental lineage relationships in the developing human brain.

Cellular output of midgestation germinal zones

To fate map the human VZ and OSVZ niches, we prepared organotypic slice cultures of primary human neocortex from gestational weeks (GW) 18-23 to capture the time point shortly after tRG emergence (3) and right at the onset of astrogliogenesis (13). We labeled these niches in paired slices from the same individual using local delivery of viral vectors expressing green fluorescent protein (GFP) under the CMV/chicken β-actin (CAG) promoter (Fig. 1A). Two days after labeling–the earliest time point at which the GFP can be detected– GFP$^+$ cells labeled by VZ infections were found in the SOX2^{dense}, CRYAB$^+$ VZ and adjacent inner subventricular zone, while cells labeled by OSVZ infections were located in the SOX2^{dense}, CRYAB$^-$ OSVZ with a few cells in the adjacent SOX2^{sparse}, CRYAB$^-$ subplate (SP) (Fig. 1B, Fig. S1A). To determine the identity of these initially labeled cells, we stained for several markers of progenitor cell subtypes (Fig. 1C–F, Fig. S1B–C). Across slices from three individuals, 76% (SD ±10%) of the cells labeled by VZ infection were SOX2$^+$ progenitors, and 10% (SD ±2%) were CRYAB$^+$ tRG (Fig. 1E). After OSVZ labeling, we found that an average of 55% (SD ±8%) of OSVZ infected GFP$^+$ cells were dividing or newly born cells that incorporated 5-bromo-2'-deoxyuridine (BrdU), and that

10% (SD ±4%) were EOMES$^+$ neuronal progenitor cells and 5% (±2%) were HOPX$^+$ oRGs (Fig. 1F). Together, this data demonstrates that our local infections are spatially specific and label progenitor cells.

Next, we compared the distributions of VZ- and OSVZ-derived cells across the VZ, SVZ, SP, and cortical plate (CP) (Fig. S2A) after 8-12 days in culture (Fig. 1G, Fig. S2C–C). Consistent with prior studies (9, 12, 14, 15), both the VZ- and OSVZ gave rise to cells with neuronal and glial morphologies (Fig. 1H–K). However, across 4-5 individuals OSVZ-derived glia largely remained within the SVZ, while VZ-derived glia were found throughout the cortical wall (Fig. 1L). To confirm that this phenotype was not induced by the serum in our culture media, we repeated this experiment in serum-free conditions and found a similar distribution (Fig. S3). To confirm that this observation was not the result of non-specific labeling during the initial VZ infection, we labeled the VZ using an alternative method of microdissecting out the VZ, separately bathing it in virus, and then co-culturing it with the remaining tissue slice (Fig. S4A). After thirteen days in culture, the transplanted VZ gave rise to GFP$^+$ cells with both neuronal and glial morphologies (Fig. S4B–I), and the VZ-derived glial cell population was evenly distributed across all laminae (Fig. S4J). Together, our data suggest that the VZ and OSVZ give rise to distinct subpopulations of glial cells with distinct localizations within the developing cortex (Fig. 1N).

Differential distribution of astrocytes and oligodendrocytes

Next, we used co-immunostaining to determine whether this differential glial distribution could be attributed to molecularly defined astrocytes (SOX9$^+$/OLIG2$^-$), oligodendrocyte progenitor cells (OPCs, SOX9$^+$/OLIG2$^+$), and/or oligodendrocytes (SOX9$^-$/OLIG2$^+$) (Fig. 2A). We found that all three glial cell types derived from the same niche shared comparable distribution patterns (Fig. 2B), indicating that this differential glial output is a broad feature of midgestation gliogenesis. These distribution patterns were also different from those of interneurons (Fig. S5C), excitatory neurons (Fig. S5C), or all cells (Fig. S5E). However, we also found a unique enrichment of astrocytes in the CP of VZ-labeled slices compared to OSVZ-labeled that did not apply to OPCs or oligodendrocytes (Fig. 2C, Fig. S5D). Thus, while the differential glial output of VZ and OSVZ niches extends to all macroglial cell types, there is a unique enrichment of VZ-derived astrocytes in the CP (Fig. 2D).

To further confirm that the lack of OSVZ-derived glial migration was not due to a broader disruption of normal radial migration in our slice culture model, we determined the distribution of neuronal subtypes by staining for the glutamatergic neuron markers NEUROD2 and TBR1 and the GABAergic neuron marker DLX2 (Fig. S5A). We found that DLX2$^+$ cortical interneurons composed a relatively small proportion of GFP$^+$ cells in both VZ and OSVZ infections (Fig. S5B) but that they successfully migrated radially from their niche of origin (Fig. S5C). Culture in the presence of BrdU revealed BrdU$^+$ GFP$^+$/DLX2$^+$ interneurons derived from both VZ and OSVZ labeling (Fig. S5F), consistent with their dual origin in cortical and subcortical germinal zones in humans (16, 17). By contrast, the majority of GFP$^+$ cells derived from VZ or OSVZ labeling were NEUROD2$^+$ glutamatergic neurons (Fig. S5B) that migrated radially outward from their niche of origin (Fig. S5C), and included both BrdU$^-$ and newborn BrdU$^+$ GFP$^+$/TBR1$^+$ glutamatergic neurons (Fig. S5G).

Taken together, these findings demonstrates that extensive neuronal migration in our slice cultures are consistent with the expected distributions, indicating that the slice culture model can support normal patterns of cellular migration.

Morphological analysis of glial cell types

Radial glia and astrocytes undergo morphological transitions across their maturation trajectory, and morphology is a critical feature used to identify astrocyte subtypes in the absence of robust molecular markers (18). To determine whether VZ and OSVZ derived glia are morphologically heterogeneous, we analyzed the morphology of 524 randomly selected cells with glial morphology across four replicates of paired VZ- and OSVZ-labeled slices from GW20-GW23. We classified these cells into 'morphotypes' based on three previously described criteria: 1) the length of their primary processes, 2) the density of their primary processes, and 3) the types of varicosities along their processes (Table S1). This morphometric analysis resulted in the identification of 12 glial morphotypes (Fig. 3A, Fig. S6) that are consistent with previous morphology annotations at similar ages (18–20).

We observed expected radial glial morphotypes including radial glia with a single apical process (21) (Fig. 3A, Fig. S6: "radial glia-no radial processes") that were derived from and resided in the VZ of younger samples (Fig. S7A–C), as well as radial glia at various stages of transforming into astrocytes (Fig. 3A, Fig. S6: "radial glia-short radial processes" and "radial glia-long radial processes") and oRG-like cells with both apical and basal fibers (Fig. 3A, Fig. S6: "radial glia-two long processes") derived from and residing in the SVZ of older samples (Fig. S7A–C) (12). We also observed $SOX9^+/OLIG2^+/PDGFRA^+$ OPCs with few, smooth processes (Fig. 3A, Fig. S6, Fig. S8A: "sparse smooth processes") (22), and $SOX9^-/OLIG2^+/SOX10^+$ immature oligodendrocytes with many short, branched processes (Fig. 3A, Fig. S6, Fig. S8B: "bushy processes") (22). A subset of cells with "bushy processes" were also beginning to express the mature oligodendrocyte marker MBP (Fig. S8C). These putative oligodendrocyte lineage cells were derived from both the VZ and OSVZ and found across the cortical wall of all ages studied (Fig. S7A–C).

Lineage divergence of morphologically distinct astrocytes

The remaining morphotypes that did not possess a primary fiber and did not express OLIG2 represent our putative astrocyte subtypes. These morphotypes included several categories with a sparser arbor of primary processes: those with "short processes", those with "sparse beady processes" defined by long thin processes with small regularly-sized and spaced swellings, and those with "sparse processes with irregular varicosities" defined by larger and more irregularly-sized and spaced varicosities (Fig 3A, Fig S6). These morphotypes were derived from both VZ and OSVZ labeling and found in multiple layers of the cortical wall (Fig. S7B–C).

Cells with a dense arbor of primary processes fell into three subcategories: "dense bulbous processes" with large bulbous varicosities along their processses, "dense smooth processes" with few varicosities, and "dense beady processes" with regularly spaced beady varicosities (Fig. 3A, Fig. S6). The "dense bulbous processes" and "dense smooth

processes" morphotypes were unique in that they demonstrated a bias towards a single niche of origin and laminar localization. Across four individuals, 82% (SD ±13%) of astrocytes with "dense smooth processes" were derived from OSVZ labeling (Fig. 3B) and 78% (SD ±10%) remained in the SVZ (Fig. 3C) where they represented the dominant astrocyte morphotype (Fig. 3D, Fig. S7D). Gamma retrovirus labeling (Fig. S10) and BrdU incorporation experiments (Fig. 3E) demonstrated that the majority (70%, SD±13%) of these cells were born during the culture period (Fig. S7E), indicating that their lack of migration out of the SVZ was not due to labeling of mature cells. By contrast, 100% of "dense bulbous" astrocytes were derived from VZ labeling and BrdU incorporation confirmed they were born in this niche (Fig. 3B). The majority of these cells (70%, SD ±12%) were located in the CP (Fig. 3C) where they also composed the dominant morphotype (Fig. 3D), in addition to 29% (SD ±12%) in the SP (Fig. 3C). A subset of cells of this morphotype expressed AQP4 consistent with their astrocytic identity, and a subset were positive for Ki67 (Fig. S9), indicating that they could act as a locally dividing progenitor population (23). Finally, we confirmed that neither of these morphotypes were induced by our culture conditions by replicating our findings in serum-free media (Fig. S3). Together, this analysis demonstrates that during midgestation the VZ- and OSVZ give rise to astrocytes with distinct morphologies and laminar positions within the developing cerebral cortex (Fig. 3F).

Molecular characterization of astrocyte morphotypes

Finally, we sought to determine the molecular distinctions between VZ-derived "dense bulbous" and OSVZ-derived "dense smooth" astrocytes. To make this comparison we used a modified version of the recently published Patch-seq protocol (22) to use a micropipette to collect the mRNA from morphologically defined cells followed by whole transcriptome single cell sequencing (Fig 4A, Fig. S11A). Across 10 individuals, we generated Patch-seq data for 28 "dense bulbous" astrocytes, 20 "dense smooth" astrocytes, and 22 neurons to serve as an outgroup. After quality control filtering (see methods) (Fig. S11B–D), we refined our dataset down to 12 dense bulbous astrocytes, 13 dense smooth astrocytes, 3 dividing astrocytes, 6 excitatory neurons, and 8 inhibitory neurons of high quality (Fig. 4B). We then performed differential gene expression analysis to identify 445 genes differentially enriched in "dense bulbous" astrocytes or "dense smooth" astrocytes (Fig. 4C, Fig. S11E). To identify the genes that most likely mark these cell types across their lifespan, we cross referenced our differentially expressed gene list with their expression in published single cell RNA-sequencing from either the developing (24) or adult (25) human neocortex (Fig. S11F–G). This analysis highlighted ITGB4 and ANGPTL4 as candidate markers of dense bulbous and dense smooth astrocytes, respectively, that were also enriched in astrocytes in both prenatal and adult cortex (Fig. 4D). Finally, we confirmed this prediction by performing *in situ* hybridization on cultured VZ- or OSVZ-labeled slices. This work demonstrated that *ITGB4* mRNA indeed localizes to VZ-derived dense bulbous astrocytes in the CP, and *ANGPTL4* mRNA localizes to OSVZ-derived dense smooth astrocytes in the OSVZ (Fig. 4E, Fig. 12A–C). Together, these experiments demonstrate that the two neural stem cell niches of the developing human cerebral cortex give rise to spatially, morphologically, and molecularly unique astrocyte subtypes (Fig. 4H).

Discussion

Our study illuminates early developmental events that underlie the emergence of human neocortical astrocyte diversity. We find that during midgestation, OSVZ progenitor cells give rise to white matter astrocytes, while VZ progenitors give rise to more superficial gray matter astrocytes. This differentiation pattern differs from neurogenesis, where OSVZ progenitors give rise to neurons destined for the upper cortical layers. Because neurogenesis and gliogenesis overlap extensively in humans (26), unlike in rodents (27), further studies will be needed to determine if individual human progenitors can give rise to both neuronal and glial cells during this time period or follow a classical neurogenic to gliogenic 'switch', and whether these patterns of differentiation are maintained throughout development. Our study also implicates truncated radial glia (3), which have not been described in mice, in the generation of a distinct subtype of cortical "dense bulbous" astrocytes that have been previously observed in humans (20, 28), but not in rodents. Additional studies are needed to determine the developmental origin of other astrocyte subtypes thought to be enriched in humans, such as varicose projection and interlaminar astrocytes (29, 30).

Astrocytes have been increasingly implicated in neurological disease (31, 32), with distinct astrocyte subtypes being implicated in schizophrenia, bipolar disorder (33), and autism spectrum disorders (25). Molecular distinctions between white matter and gray matter astrocytes identified in this study may enable insights into their unique developmental features and disease implications. For example, many genes enriched in "dense bulbous" astrocytes have been implicated in glioblastoma cell proliferation and invasion, such as *ITGB4* (34), *TMEM158* (35), *MGMT* (36), and *CELSR1* (37), which could explain their remarkable migratory behavior. Detailed mapping of the developmental trajectories of these early astrocyte subtypes through the third trimester and into adulthood will be important to determine whether this astrocyte diversity is encoded at the level of progenitors or dynamically influenced by environmental cues present in distinct brain regions or cellular neighborhoods. In turn, these studies may reveal important subtype-specific vulnerabilities to environmental or genetic insults that underlie this diverse role for astrocytes in neurological disease.

Supplementary Material

Refer to Web version on PubMed Central for supplementary material.

Acknowledgements:

Data and materials availability:

Morphology classification data is provided in Supplementary Table 1. Patch-seq counts are provided in Supplementary Table 2 and corresponding metadata are provided in Supplementary Table 3. Code used to generate the data is available at the Github repository: https://zenodo.org/badge/latestdoi/471078301. Materials requests should be addressed to TJN.

References

1. Cadwell CR, Bhaduri A, Mostajo-Radji MA, Keefe MG, Nowakowski TJ, Development and Arealization of the Cerebral Cortex. Neuron. 103, 980–1004 (2019). [PubMed: 31557462]

2. Libé-Philippot B, Vanderhaeghen P, Cellular and Molecular Mechanisms Linking Human Cortical Development and Evolution. Annu. Rev. Genet 55, 555–581 (2021). [PubMed: 34535062]

3. Nowakowski TJ, Pollen AA, Sandoval-Espinosa C, Kriegstein AR, Transformation of the Radial Glia Scaffold Demarcates Two Stages of Human Cerebral Cortex Development. Neuron. 91, 1219–1227 (2016). [PubMed: 27657449]

4. Taverna E, Götz M, Huttner WB, The cell biology of neurogenesis: toward an understanding of the development and evolution of the neocortex. Annu. Rev. Cell Dev. Biol 30, 465–502 (2014). [PubMed: 25000993]

5. Kalebic N, Gilardi C, Stepien B, Wilsch-Bräuninger M, Long KR, Namba T, Florio M, Langen B, Lombardot B, Shevchenko A, Kilimann MW, Kawasaki H, Wimberger P, Huttner WB, Neocortical Expansion Due to Increased Proliferation of Basal Progenitors Is Linked to Changes in Their Morphology. Cell Stem Cell. 24, 535–550.e9 (2019). [PubMed: 30905618]

6. Kalebic N, Huttner WB, Basal Progenitor Morphology and Neocortex Evolution. Trends Neurosci. 43, 843–853 (2020). [PubMed: 32828546]

7. Fietz SA, Kelava I, Vogt J, Wilsch-Bräuninger M, Stenzel D, Fish JL, Corbeil D, Riehn A, Distler W, Nitsch R, Huttner WB, OSVZ progenitors of human and ferret neocortex are epithelial-like and expand by integrin signaling. Nat. Neurosci 13, 690–699 (2010). [PubMed: 20436478]

8. Smart IHM, Dehay C, Giroud P, Berland M, Kennedy H, Unique morphological features of the proliferative zones and postmitotic compartments of the neural epithelium giving rise to striate and extrastriate cortex in the monkey. Cereb. Cortex 12, 37–53 (2002). [PubMed: 11734531]

9. Hansen DV, Lui JH, Parker PRL, Kriegstein AR, Neurogenic radial glia in the outer subventricular zone of human neocortex. Nature. 464, 554–561 (2010). [PubMed: 20154730]

10. Reillo I, de Juan Romero C, García-Cabezas MÁ, Borrell V, A role for intermediate radial glia in the tangential expansion of the mammalian cerebral cortex. Cereb. Cortex 21, 1674–1694 (2011). [PubMed: 21127018]

11. Pollen AA, Nowakowski TJ, Chen J, Retallack H, Sandoval-Espinosa C, Nicholas CR, Shuga J, Liu SJ, Oldham MC, Diaz A, Lim DA, Leyrat AA, West JA, Kriegstein AR, Molecular identity of human outer radial glia during cortical development. Cell. 163, 55–67 (2015). [PubMed: 26406371]

12. Betizeau M, Cortay V, Patti D, Pfister S, Gautier E, Bellemin-Ménard A, Afanassieff M, Huissoud C, Douglas RJ, Kennedy H, Dehay C, Precursor diversity and complexity of lineage relationships in the outer subventricular zone of the primate. Neuron. 80, 442–457 (2013). [PubMed: 24139044]

13. deAzevedo LC, Fallet C, Moura-Neto V, Daumas-Duport C, Hedin-Pereira C, Lent R, Cortical radial glial cells in human fetuses: depth-correlated transformation into astrocytes. J. Neurobiol 55, 288–298 (2003). [PubMed: 12717699]

14. Rash BG, Duque A, Morozov YM, Arellano JI, Micali N, Rakic P, Gliogenesis in the outer subventricular zone promotes enlargement and gyrification of the primate cerebrum. Proc. Natl. Acad. Sci. U. S. A 116, 7089–7094 (2019). [PubMed: 30894491]

15. Huang W, Bhaduri A, Velmeshev D, Wang S, Wang L, Rottkamp CA, Alvarez-Buylla A, Rowitch DH, Kriegstein AR, Origins and Proliferative States of Human Oligodendrocyte Precursor Cells. Cell. 182, 594–608.e11 (2020). [PubMed: 32679030]

16. Marín O, Rubenstein JL, A long, remarkable journey: tangential migration in the telencephalon. Nat. Rev. Neurosci 2, 780–790 (2001). [PubMed: 11715055]

17. Delgado RN, Allen DE, Keefe MG, Mancia Leon WR, Ziffra RS, Crouch EE, Alvarez-Buylla A, Nowakowski TJ, Individual human cortical progenitors can produce excitatory and inhibitory neurons. Nature. 601, 397–403 (2022). [PubMed: 34912114]

18. Marín-Padilla M, Prenatal development of fibrous (white matter), protoplasmic (gray matter), and layer I astrocytes in the human cerebral cortex: a Golgi study. J. Comp. Neurol 357, 554–572 (1995). [PubMed: 7545703]

19. Falcone C, Penna E, Hong T, Tarantal AF, Hof PR, Hopkins WD, Sherwood CC, Noctor SC, Martínez-Cerdeño V, Cortical Interlaminar Astrocytes Are Generated Prenatally, Mature Postnatally, and Express Unique Markers in Human and Nonhuman Primates. Cereb. Cortex 31, 379–395 (2021). [PubMed: 32930323]

20. Akiyama H, Tooyama I, Kawamata T, Ikeda K, McGeer PL, Morphological diversities of CD44 positive astrocytes in the cerebral cortex of normal subjects and patients with Alzheimer's disease. Brain Res. 632, 249–259 (1993). [PubMed: 7511977]

21. Schmechel DE, Rakic P, A Golgi study of radial glial cells in developing monkey telencephalon: morphogenesis and transformation into astrocytes. Anat. Embryol . 156, 115–152 (1979).

22. Bergles DE, Richardson WD, Oligodendrocyte Development and Plasticity. Cold Spring Harb. Perspect. Biol 8, a020453 (2015). [PubMed: 26492571]

23. Ge W-P, Miyawaki A, Gage FH, Jan YN, Jan LY, Local generation of glia is a major astrocyte source in postnatal cortex. Nature. 484, 376–380 (2012). [PubMed: 22456708]

24. Bhaduri A, Sandoval-Espinosa C, Otero-Garcia M, Oh I, Yin R, Eze UC, Nowakowski TJ, Kriegstein AR, An atlas of cortical arealization identifies dynamic molecular signatures. Nature. 598, 200–204 (2021). [PubMed: 34616070]

25. Velmeshev D, Schirmer L, Jung D, Haeussler M, Perez Y, Mayer S, Bhaduri A, Goyal N, Rowitch DH, Kriegstein AR, Single-cell genomics identifies cell type-specific molecular changes in autism. Science. 364, 685–689 (2019). [PubMed: 31097668]

26. Malik S, Vinukonda G, Vose LR, Diamond D, Bhimavarapu BBR, Hu F, Zia MT, Hevner R, Zecevic N, Ballabh P, Neurogenesis continues in the third trimester of pregnancy and is suppressed by premature birth. J. Neurosci 33, 411–423 (2013). [PubMed: 23303921]

27. Noctor SC, Martínez-Cerdeño V, Ivic L, Kriegstein AR, Cortical neurons arise in symmetric and asymmetric division zones and migrate through specific phases. Nat. Neurosci 7, 136–144 (2004). [PubMed: 14703572]

28. Matyash V, Kettenmann H, Heterogeneity in astrocyte morphology and physiology. Brain Res. Rev 63, 2–10 (2010). [PubMed: 20005253]

29. Falcone C, McBride EL, Hopkins WD, Hof PR, Manger PR, Sherwood CC, Noctor SC, Martínez-Cerdeño V, Redefining varicose projection astrocytes in primates. Glia. 70, 145–154 (2022). [PubMed: 34533866]

30. Falcone C, Wolf-Ochoa M, Amina S, Hong T, Vakilzadeh G, Hopkins WD, Hof PR, Sherwood CC, Manger PR, Noctor SC, Martínez-Cerdeño V, Cortical interlaminar astrocytes across the therian mammal radiation. J. Comp. Neurol 527, 1654–1674 (2019). [PubMed: 30552685]

31. Lee H-G, Wheeler MA, Quintana FJ, Function and therapeutic value of astrocytes in neurological diseases. Nat. Rev. Drug Discov (2022), doi:10.1038/s41573-022-00390-x.

32. Guttenplan KA, Weigel MK, Prakash P, Wijewardhane PR, Hasel P, Rufen-Blanchette U, Münch AE, Blum JA, Fine J, Neal MC, Bruce KD, Gitler AD, Chopra G, Liddelow SA, Barres BA, Neurotoxic reactive astrocytes induce cell death via saturated lipids. Nature. 599, 102–107 (2021). [PubMed: 34616039]

33. Hercher C, Chopra V, Beasley CL, Evidence for morphological alterations in prefrontal white matter glia in schizophrenia and bipolar disorder. J. Psychiatry Neurosci 39, 376–385 (2014). [PubMed: 24936776]

34. Hu Y, Ylivinkka I, Chen P, Li L, Hautaniemi S, Nyman TA, Keski-Oja J, Hyytiäinen M, Netrin-4 promotes glioblastoma cell proliferation through integrin β4 signaling. Neoplasia. 14, 219–227 (2012). [PubMed: 22496621]

35. Li J, Wang X, Chen L, Zhang J, Zhang Y, Ren X, Sun J, Fan X, Fan J, Li T, Tong L, Yi L, Chen L, Liu J, Shang G, Ren X, Zhang H, Yu S, Ming H, Huang Q, Dong J, Zhang C, Yang X, TMEM158 promotes the proliferation and migration of glioma cells via STAT3 signaling in glioblastomas. Cancer Gene Ther. (2022), doi:10.1038/s41417-021-00414-5.

36. Hegi ME, Diserens A-C, Gorlia T, Hamou M-F, de Tribolet N, Weller M, Kros JM, Hainfellner JA, Mason W, Mariani L, Bromberg JEC, Hau P, Mirimanoff RO, Cairncross JG, Janzer RC, Stupp R, MGMT gene silencing and benefit from temozolomide in glioblastoma. N. Engl. J. Med 352, 997–1003 (2005). [PubMed: 15758010]

37. Wang G, Li Y, Zhang D, Zhao S, Zhang Q, Luo C, Sun X, Zhang B, CELSR1 Acts as an Oncogene Regulated by miR-199a-5p in Glioma. Cancer Manag. Res 12, 8857–8865 (2020). [PubMed: 33061581]

38. Rakic P, Neuron-glia relationship during granule cell migration in developing cerebellar cortex. A Golgi and electronmicroscopic study in Macacus Rhesus. J. Comp. Neurol 141, 283–312 (1971). [PubMed: 4101340]

39. Oberheim NA, Takano T, Han X, He W, Lin JHC, Wang F, Xu Q, Wyatt JD, Pilcher W, Ojemann JG, Ransom BR, Goldman SA, Nedergaard M, Uniquely hominid features of adult human astrocytes. J. Neurosci 29, 3276–3287 (2009). [PubMed: 19279265]

40. Cadwell CR, Scala F, Li S, Livrizzi G, Shen S, Sandberg R, Jiang X, Tolias AS, Multimodal profiling of single-cell morphology, electrophysiology, and gene expression using Patch-seq. Nat. Protoc 12, 2531–2553 (2017). [PubMed: 29189773]

41. Bardy C, van den Hurk M, Kakaradov B, Erwin JA, Jaeger BN, Hernandez RV, Eames T, Paucar AA, Gorris M, Marchand C, Jappelli R, Barron J, Bryant AK, Kellogg M, Lasken RS, Rutten BPF, Steinbusch HWM, Yeo GW, Gage FH, Predicting the functional states of human iPSC-derived neurons with single-cell RNA-seq and electrophysiology. Mol. Psychiatry 21, 1573–1588 (2016). [PubMed: 27698428]

42. Tripathy SJ, Toker L, Bomkamp C, Mancarci BO, Belmadani M, Pavlidis P, Assessing Transcriptome Quality in Patch-Seq Datasets. Front. Mol. Neurosci 11, 363 (2018). [PubMed: 30349457]
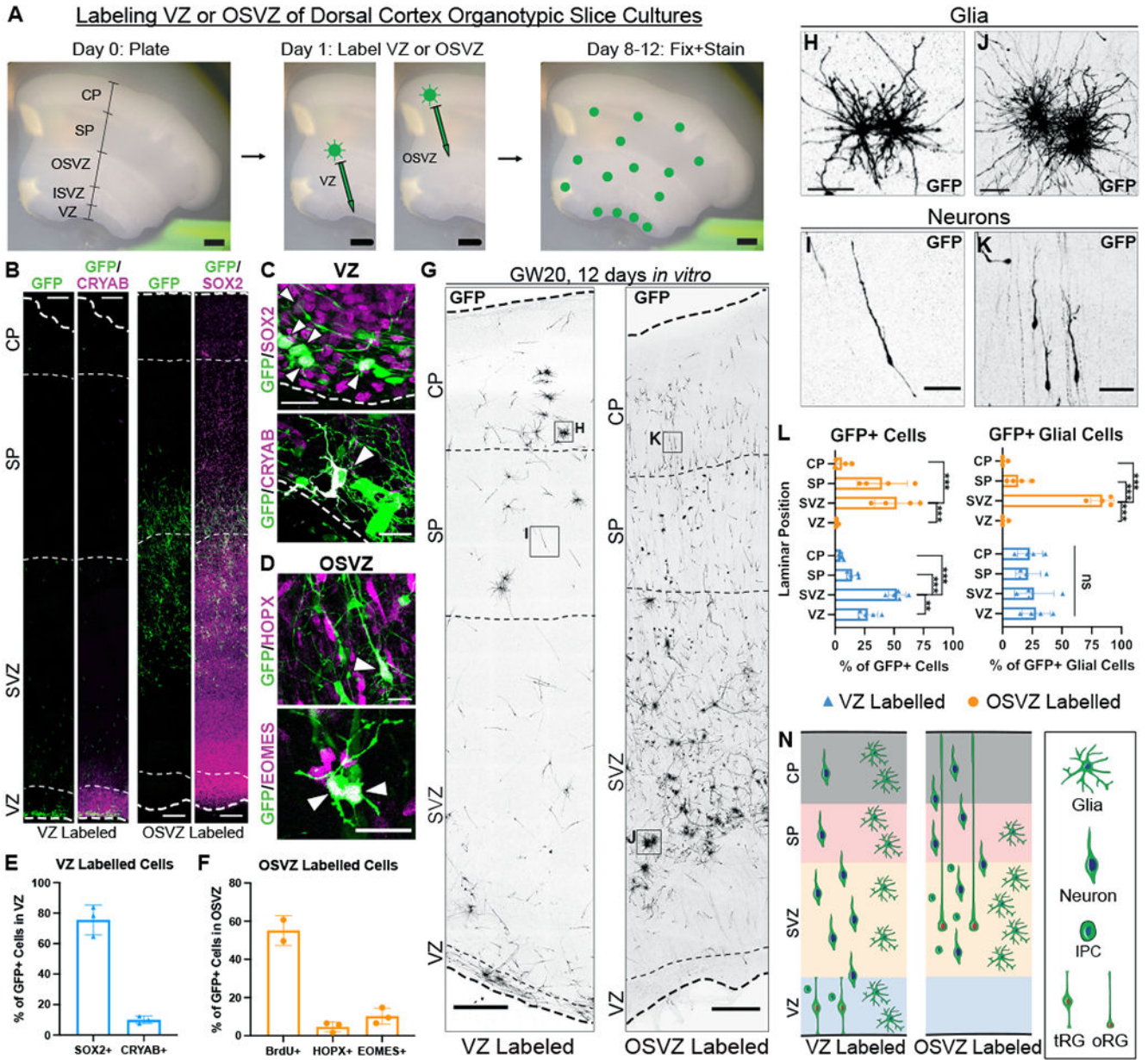
**Figure 1: VZ and OSVZ niches both give rise to neurons but contribute distinct populations of glia.**

(**A**) Schematic of experimental design. VZ and OSVZ are visualized on a dissection microscope, virus is applied to the VZ or OSVZ using a glass needle, and after 8-12 days labeled GFP+ cells (green dots) have migrated throughout the slice. Scale bar = 1mm. (**B**) GW19 sample 2 days after VZ or OSVZ labeling co-immunostained for GFP and CRYAB or SOX2. Thick dashed lines indicate ventricular and pial edges, thin dashed lines indicate borders between laminae. Scale bars = 250μm. (**C**) GFP+/SOX2+ or GFP+/CRYAB+ cells in the VZ 2 days after VZ labeling. White arrowheads indicate double-positive cells. Scale bar = 25μm. **D)** GFP+/HOPX+ or GFP+/EOMES+ cells in the OSVZ 2 days after OSVZ labeling. White arrowheads indicate double-positive cells. Scale bar = 25μm. **E)**

Quantification (mean±SD) of the percentage of GFP$^+$ cells in the VZ that are SOX2$^+$ or CRYAB$^+$ 2 days after VZ labeling. N=3 independent samples. **F)** Quantification (mean±SD) of the percentage of GFP+ cells in the OSVZ that are BrdU$^+$, HOPX$^+$, or EOMES$^+$ 2 days after OSVZ labeling. N=2-3 independent samples. **G)** GFP immunostaining of GW20 sample 12 days after VZ or OSVZ labeling. Dashed lines as in (B). Scale bar = 500um. (**H-K**) Insets from (G) showing cells with glial morphology (H, J) and neuronal morphology (I, K). Scale bars = 50μm. (**L**) Quantification (mean±SD) of the percentage of total VZ- or OSVZ-derived GFP$^+$ cells or GFP$^+$ cells with glial morphology located in each lamina of the developing cortex at the end of culture (n=4-5 independent samples). Laminar borders were determined using DAPI density (Fig. S2A). Statistical significance assessed with one-way analysis of variance (ANOVA) with Tukey's multiple comparisons correction. *: $q < 0.033$, **: $q < 0.002$, ***: $q < 0.001$ ns: not significant. (**N**) Schematic summarizing distribution of VZ- or OSVZ-derived cells.
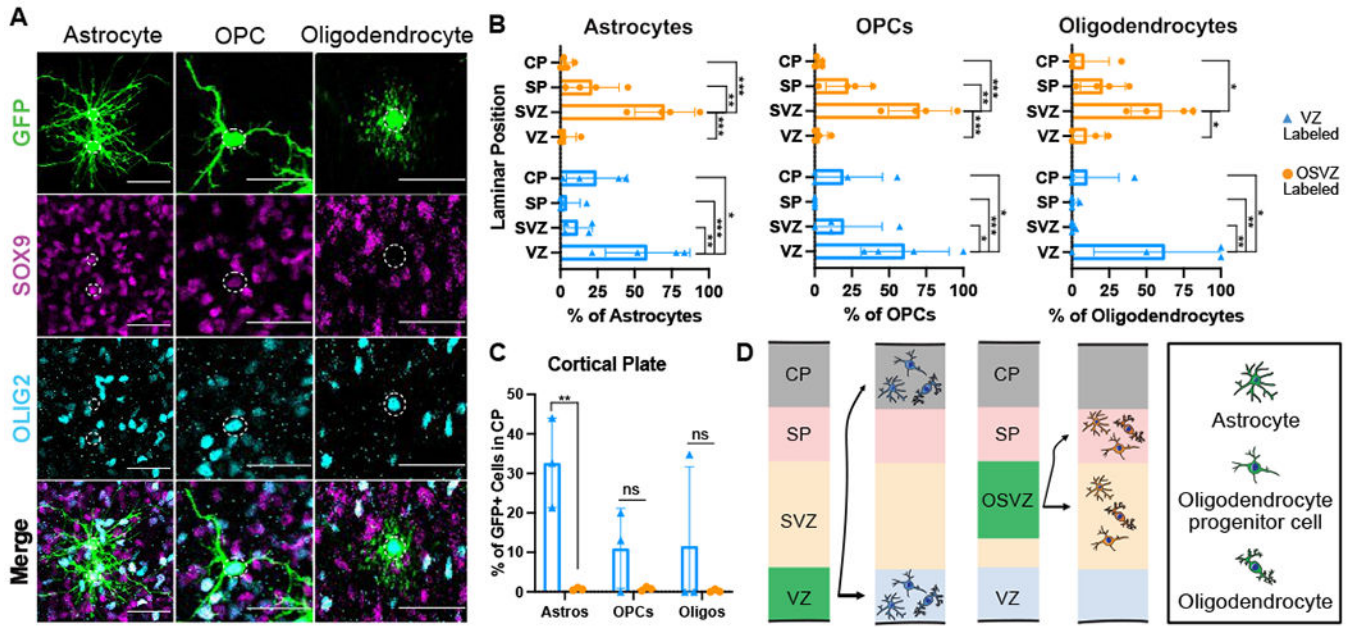
Figure 2: VZ and OSVZ give rise to spatially distinct populations of astrocytes, OPCs, and oligodendrocytes.

(**A**) Co-immunostaining showing representative GFP+/SOX9+/OLIG2− astrocytes, GFP+/SOX9+/OLIG2+ OPC, and GFP+/SOX9−/OLIG2+ oligodendrocyte. All scale bars = 50μm. (**B**) Quantification (mean±SD) of the percentage of VZ- or OSVZ-derived astrocytes, OPCs, or oligodendrocytes that were located in the VZ, SVZ, SP, or CP at the end of culture. N=4 independent samples for all. (**C**) Quantification (mean±SD) of the percentage of total GFP+ cells in the CP of VZ- or OSVZ-labeled slices that were astrocytes (Astros), OPCs, or oligodendrocytes (Oligos). N=3 independent samples. All statistical significance assessed with two-way ANOVA with Tukey's multiple comparison test correction. *: q < 0.033, **: q < 0.002, ***: q < 0.001 ns: not significant. (**D**) Schematic summarizing the distinct distribution of VZ versus OSVZ-derived astrocytes, OPCs, and oligodendrocytes. Green color indicates the niche of origin. Arrow line weight corresponds to relative abundance in the target layer.
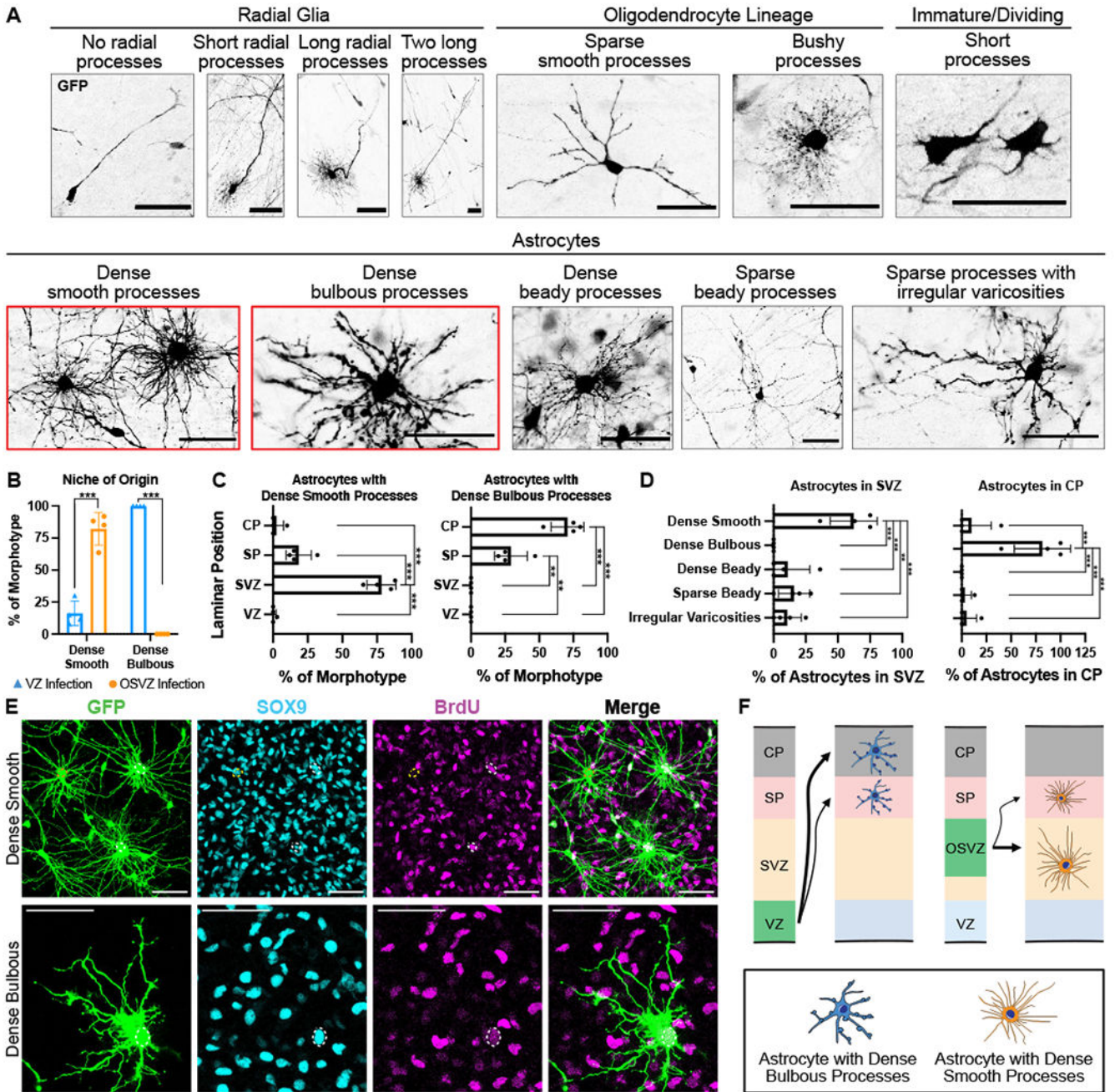
Figure 3: VZ and OSVZ give rise to morphologically distinct astrocyte subtypes.
(**A**) GFP immunostaining showing representative images of the twelve glial morphotypes identified in this study. Scale bars = 50μm. Red boxes outline morphotypes analyzed later in the figure. (**B**) Quantification (mean±SD) of the percentage of astrocytes with dense smooth or dense bulbous processes derived from VZ or OSVZ labeling. (**C**) Quantification (mean±SD) of the percentage of astrocytes with dense smooth or dense bulbous processes located in each lamina at the end of culture. (**D**) Quantification (mean±SD) of the percentage of GFP+ astrocytes within the SVZ or CP that adopted each of our five identified astrocyte morphologies. Statistical significance assessed with one or two-way ANOVA with

Tukey's multiple comparison correction. *: q < 0.033, **: q < 0.002, ***: q < 0.001 ns: not significant. N=4 independent pairs of VZ and OSVZ infections for (B-D). (**E**) Representative images of GFP⁺/SOX9⁺ "dense smooth" or "dense bulbous" astrocytes that are BrdU⁺ (white dashed outline) or BrdU⁻(yellow dashed outline). Scale bar = 50μm. (**F**) Schematic summarizing the differential contribution of the VZ and OSVZ to astrocyte morphotypes. Arrow line weight corresponds to relative contribution to the target layer of the cortical wall.
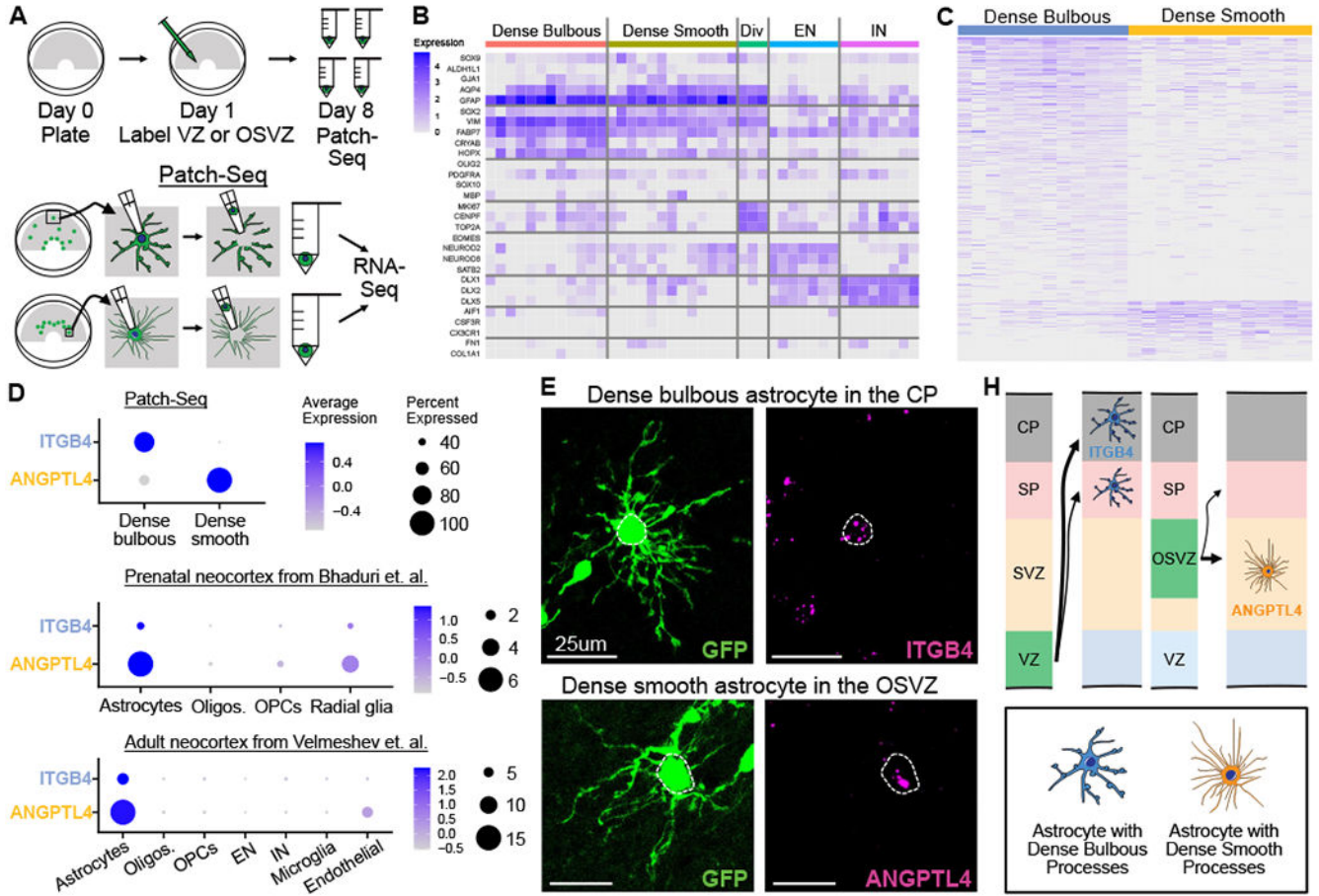
Figure 4: "Dense bulbous" and "dense smooth" astrocytes have unique molecular profiles.
(**A**) Schematic depicting the collection of mRNA from morphologically-defined astrocyte morphotypes using Patch-seq. (**B**) Heatmap depicting expression of major cell type marker genes across the 45 cells collected by Patch-seq and used for further analysis. Horizontal gray lines indicate the borders between expression of markers of astrocytes, radial glia, oligodendrocyte lineage cells, dividing cells, excitatory neurons, inhibitory neurons, microglia, and endothelial cells. Div: Dividing cells. EN: excitatory neurons. IN: inhibitory neurons. (**C**) Heatmap depicting expression of the 445 genes differentially expressed between "dense bulbous" and "dense smooth" astrocytes (rows), plotted across the 25 astrocytes collected by Patch-seq (columns). (**D**) Dotplots depicting the expression of ITGB4 and ANGPTL4 across astrocyte morphotypes collected by patch-seq and across cell types in the prenatal or adult cortex Oligos: Oligodendrocytes; OPCs: oligodendrocyte progenitor cells; EN: excitatory neurons; IN: inhibitory neurons. (**E**) *In situ* hybridization demonstrating expression of ITGB4 in a VZ-derived dense bulbous astrocyte in the CP and ANGPTL4 expression in an OSVZ-derived dense smooth astrocyte in the OSVZ. (**H**) Schematic summarizing the contribution of VZ and OSVZ to ITGB4+ "dense bulbous" astrocytes and ANGPTL4+ "dense smooth" astrocytes.